Lithium Silicide Surface Enrichment: A Solution to Lithium Metal Battery

Wei Tang, Xuesong Yin, Sujin Kang, Zhongxin Chen, Bingbing Tian, Siew Lang Teo, Xiaowei Wang, Xiao Chi, Kian Ping Loh,* Hyun-Wook Lee,* and Guangyuan Wesley Zheng*

The propensity of lithium dendrite formation during the charging process of lithium metal batteries is linked to inhomogeneity on the lithium surface layer. The high reactivity of lithium and the complex surface structure of the native layer create "hot spots" for fast dendritic growth. Here, it is demonstrated that a fundamental restructuring of the lithium surface in the form of lithium silicide (Li_xSi) can effectively eliminate the surface inhomogeneity on the lithium surface. In situ optical microscopic study is carried out to monitor the electrochemical deposition of lithium on the Li_xSi-modified lithium electrodes and the bare lithium electrode. It is observed that a much more uniform lithium dissolution/deposition on the Li_xSi-modified lithium anode can be achieved as compared to the bare lithium electrode. Full cells paring the modified lithium anode with sulfur and $LiFePO_4$ cathodes show excellent electrochemical performances in terms of rate capability and cycle stability. Compatibility of the anode enrichment method with mass production process also offers a practical way for enabling lithium metal anode for next-generation lithium batteries.

Lithium metal is a promising anode material for the next-generation battery technologies as it has a high-specific capacity of 3860 mAh g^{-1}, which is approximately one order of magnitude higher than that of the conventional graphite anode.[1–8] In addition, the use of lithium metal anode can further expand the choice of cathode materials to include lithium-free candidates with high-specific capacities, such as V_2O_5, sulfur, and oxygen.[9–11] The specific energy densities of these batteries can be around 3–5 times of today's lithium–ion batteries.[12,13] While there have been significant progresses, the challenges for fully utilizing lithium metal as an anode in commercial cells are still immense. For example, lithium metal tends to grow a dendritic structure upon fast charging. In addition, the continuous reaction between lithium dendrite and the organic electrolyte leads to increase in impedance and results in poor Coulombic efficiency.[4,14–19] As a consequence, excess lithium metal is usually needed for lithium metal batteries. These problems boil down to the inhomogeneous solid–electrolyte interface (SEI), which results in nonuniform deposition and dissolution of lithium during the charge/discharge cycle.[20–26] Recently, there have been significant efforts in tackling the lithium metal problems. For example, various modifications have been reported to improve the specific surface area of the electrodes by using 3D current collectors, i.e., 3D porous copper,[27,28] copper nanowire mesh,[29] submicrometer skeleton of copper[30,31] and 3D frameworks of graphic carbon nanostructures,[32–37] or by building up 3D lithium-penetrated composite electrodes.[38–40] Although certain improvements in lithium anode performance have been achieved, some of these methods are difficult to scale up in practical batteries, while others involved forming lithium metal composite that significantly reduce the specific capacity of lithium metal anode. Moreover, the increased surface area may aggravate the site reaction between the electrode and electrolyte,

Dr. W. Tang, Dr. X. Yin, S. L. Teo, Prof. G. W. Zheng
Institute of Materials Research and Engineering
A*STAR
2 Fusionopolis Way, Innovis, Singapore 138634, Singapore
E-mail: wesley-zheng@imre.a-star.edu.sg

Dr. W. Tang
School of Chemical Engineering and Technology
Xi'an Jiaotong University
Xi'an, Shaanxi 710049, China

S. Kang, Prof. H.-W. Lee
School of Energy and Chemical Engineering
Ulsan National Institute of Science and Technology (UNIST)
Ulsan 44919, Republic of Korea
E-mail: hyunwooklee@unist.ac.kr

Z. Chen, X. Wang, Prof. K. P. Loh
Department of Chemistry
National University of Singapore
3 Science Drive 3, Singapore 117543, Singapore
E-mail: chmlohkp@nus.edu.sg

Prof. B. Tian
International Collaborative Laboratory of 2D Materials for
Optoelectronics Science and Technology
Key Laboratory of Optoelectronic Devices and Systems
of Ministry of Education and Guangdong Province
Shenzhen University
Shenzhen 518060, China

Dr. X. Chi
Singapore Synchrotron Light Source
National University of Singapore
Singapore 117603, Singapore

Prof. G. W. Zheng
Department of Chemical and Biomolecular Engineering
National University of Singapore
10 Kent Ridge Crescent, Singapore 119260, Singapore

resulting in the rapid degradation of battery performance. Some electrolyte additives have been reported to stabilize the lithium surface.[41,42] To obtain maximum capacity from lithium metal anode, it is best to use lithium in its original form, with the caveat that the interfacial issue on lithium has to be solved first. So far, several approaches have been explored to engineer the surface of lithium metal, such as solid-state electrolytes,[43–50] hybrid solid electrolyte,[51–55] ion-conductive polymer,[56–62] metals,[63] metal oxides,[64] 2D materials, etc.[65,66] Depositing polymeric passivation layers on lithium foil does not solve the problems at its roots because the interstitial regions between the adlayer and lithium are still prone to dendritic growth. On the other hand, the utilization of inorganic solid electrolytes is also hindered by their poor interfacial compatibility with lithium and difficulty in fabricating. Surface modification of inorganic solid electrolyte is necessary.[49] A better strategy is to construct a surface layer that provides uniform sites for lithium reaction, as well as create a buffer in electrochemical potential between the highly reducing lithium anode and the organic electrolyte.

To build up the ion-conducting layer on top of lithium foil, conformal silicon deposition was first carried out in a radio frequency (RF)-magnetron sputtering system at room temperature (**Figure 1**a-i). Upon coating with Si, the as-prepared lithium foil was transferred into the glove box and heated to 250 °C to speed up the alloying between the lithium and the deposited Si (Figure 1a-ii) to form a Li_xSi layer (Figure 1a-iii). The idea is to provide a uniform alloying layer for lithiation before lithium deposition. In a conventional pristine lithium metal anode, due to the various surface formation energies and diffusion barriers of the species on the surface,[67,68] lithium dissolution/deposition from the pristine lithium surface is generally uneven and only part of surface area is involved in the reaction process (Figure 1c). As a result, the real local current density is much higher than the intended value during the charging/discharging. Previous study has shown that a higher local current density leads to increased nucleation sites and growth of small dendrites.[69] By coating the lithium foil with a Li_xSi layer, the lithium reaction could be much more uniform and a higher percentage of the lithium surface is utilized, which can help to distribute the applied current on the whole surface (Figure 1b).

When Si is deposited onto the lithium surface, the silvery lithium foil changes into yellow (**Figure 2**a,b and Figure S1, Supporting Information). The deposited Si layer is amorphous (Figures S2 and S3, Supporting Information) and its thickness is ≈330 nm (Figure 2d). Upon heating, the Si layer is lithiated by the melted lithium, as indicated by the change in color to gray. Plane-view images of the Si-coated lithium foil (Figure 2e,f) show that the sputter-growth Si nanograins uniformly cover the
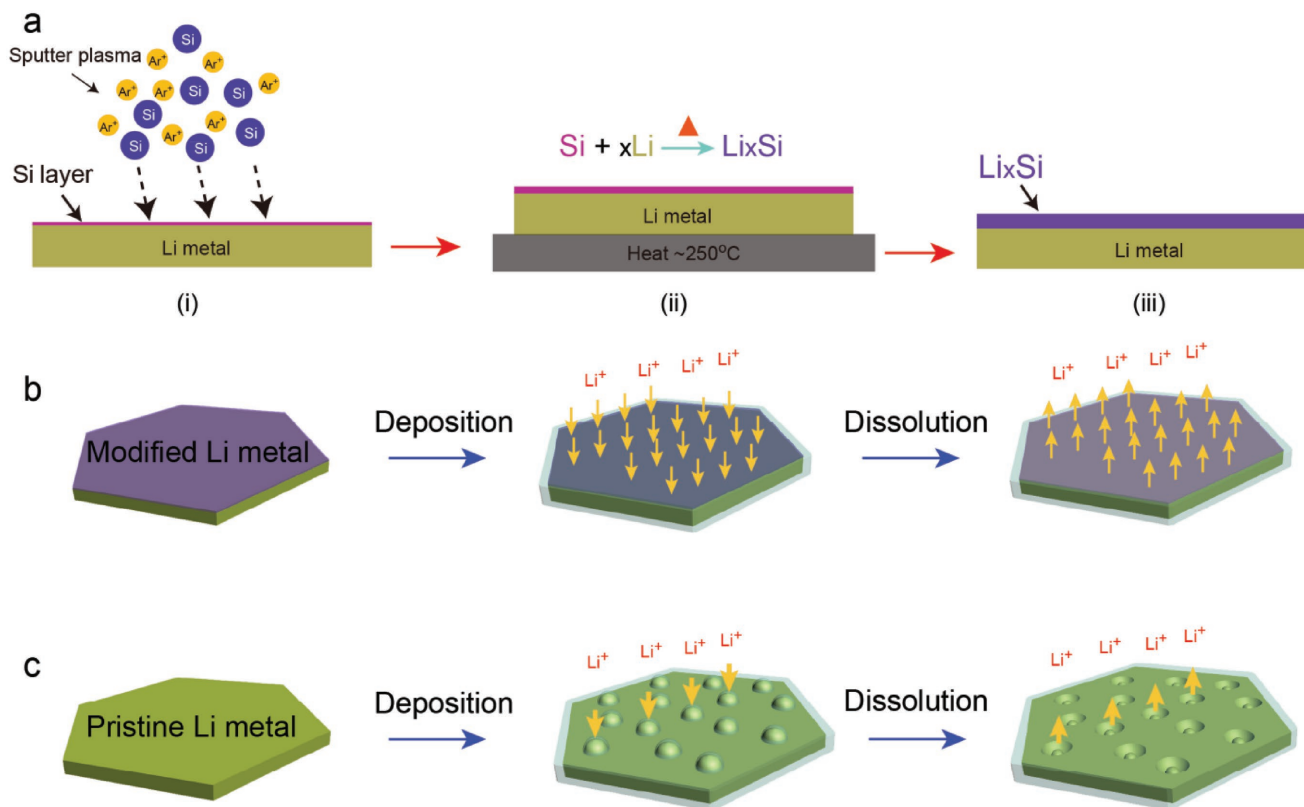

Figure 1. Schematic representation of the preparation process and electrochemical behavior of Li_xSi-modified lithium foil. a) The preparation process of Li_xSi-modified lithium foil: i) sputter-growth of thin layer of Si on lithium foil; ii) heating the Si-modified lithium foil to be the melting point of lithium metal, and iii) melted lithium reacting with Si to form Li_xSi. Illustrator of electrochemical deposition and dissolution of lithium on Li_xSi-modified b) lithium foil and c) pristine lithium foil. As shown in panel (c), the dissolution and deposition of lithium on the surface of pristine lithium is nonuniform. While only part of surface area is involved in the process, the real local current density should be much larger than the applied one. In contrary, the deposition and dissolution on the Li_xSi-modified lithium foil proceed through a uniform manner to effectively improve the utilization of lithium surface, which can help to distribute the applied current on the whole surface.
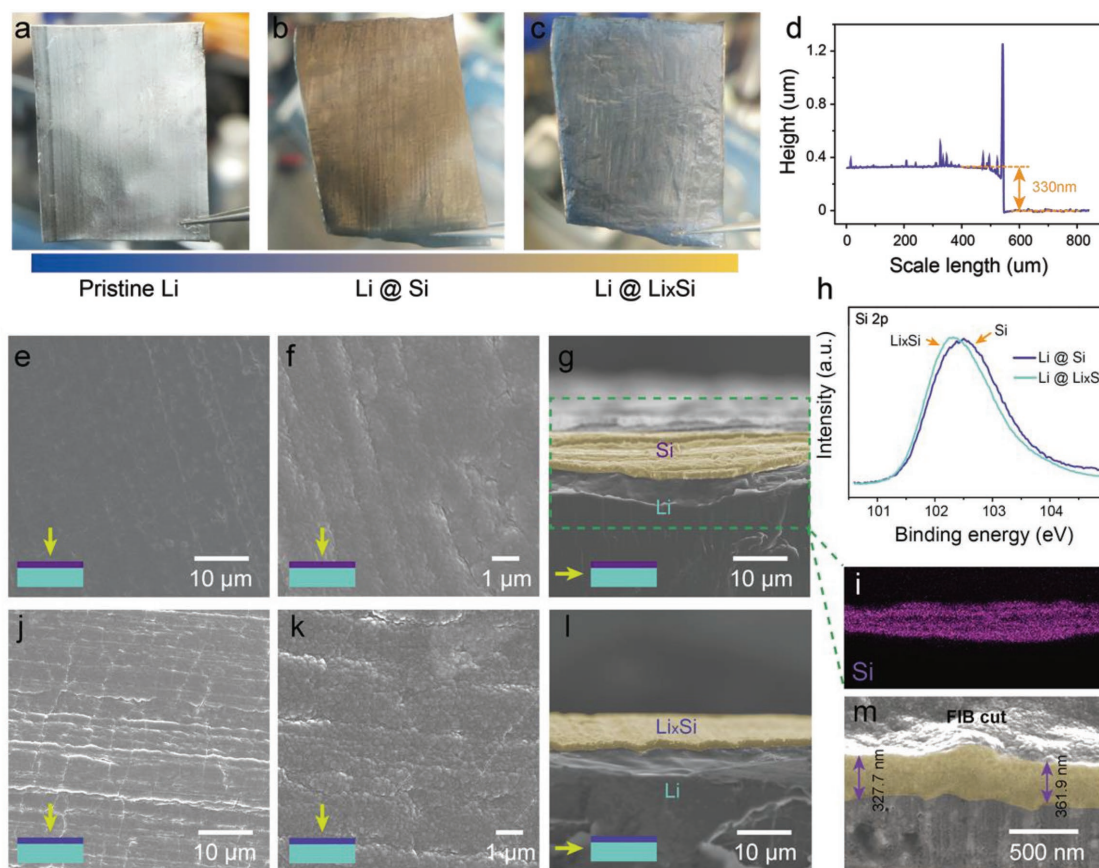
Figure 2. Characterizations of Li_xSi-modified lithium foil. Photographs of a) pristine lithium foil, b) lithium foil coated by sputter-growth Si, and c) Li_xSi; and d) surface profile of sputter-growth Si to show the thickness. SEM images of e,f) plane view and g) cross-section of Si-coated lithium foil. h) Synchrotron radiation XPS of lithium foil coated by Si and Li_xSi layer. i) EDS mapping of the cross-section of Si-coated lithium foil to show the signal of Si. SEM images of j,k) surface and l) cross-section of Li_xSi-coated lithium foil. m) SEM image of FIB cut cross-section of Li_xSi-coated lithium foil to demonstrate the thickness of coating layer.

surface of the lithium foil. The cross-section images (Figure 2g and Figure S4, Supporting Information) show a clear uniform silicon coating on top of the lithium foil [Some scanning electron microscopy (SEM) images are colored for greater clarity. The original images are shown in Figure S5 in the Supporting Information.]. From the EDS mapping (Figure 2i), Si signals are mainly observed in the coating layer, which is consistent with energy dispersive spectroscopy (EDS) spectra (Figure S6 and Table S1, Supporting Information). As calculated from the EDS, the Si content is 26.81 wt% and the oxygen content is 3.92 wt%, which indicates light surface oxidation of the Si nanograins. The Si 2p peak of Si-coated lithium foil shifts to lower binding energy, indicating the lithiation of Si by melting lithium to be Li_xSi upon heating [Figure 2h; X-ray photoelectron spectroscopy (XPS) of Li 1s peak is shown in Figure S7 in the Supporting Information.]. Upon lithiation by the melted lithium, the surface is slightly roughened due to the volumetric change of lithiated silicon, but the overall surface morphology is still quite uniform (Figure 2j,k; during the lithium deposition/dissolution, the actual volumetric variation of the protection film is quite small as shown in Figure S8 in the Supporting Information.). The coating layer is estimated to be around 350 nm, as observed from the cross-section view (Figure 2l,m).

Spatially uniform lithium transport between the electrolyte and lithium foil is important for the stable lithium deposition/dissolution.[1] To investigate the effect of the Li_xSi coating, we performed in situ optical microscopic study to monitor the electrochemical deposition of lithium on the modified and pristine lithium electrodes using a custom-made glass cell. The symmetric cell comprised of either two pristine lithium foils or two modified lithium foils as working and counter electrodes, with a piece of commercial separator soaked with electrolyte placed in the middle (**Figure 3**c,d). Using a current density of 1 mA cm^{-2}, the voltage profiles (Figure 3a) and morphological evolutions of the electrodes (Figure 3e,f) were recorded at the same time. For the control pristine lithium electrode (Figure 3e and Movie S1, Supporting Information), the morphology of lithium deposition is uneven and porous, along with obvious dendrite growth at 6 h. In contrast, the Li deposition on modified lithium electrode is relatively smooth and dense, even after 10 h of charging (Figure 3f and Movie S1, Supporting Information). The morphology evolution agrees with the voltage profile. A flat voltage profile was observed for the lithium deposition on the modified lithium electrode compared to the unstable deposition voltage profile on the pristine lithium (Figure 3a). Quantitative comparison of the morphological evolutions by
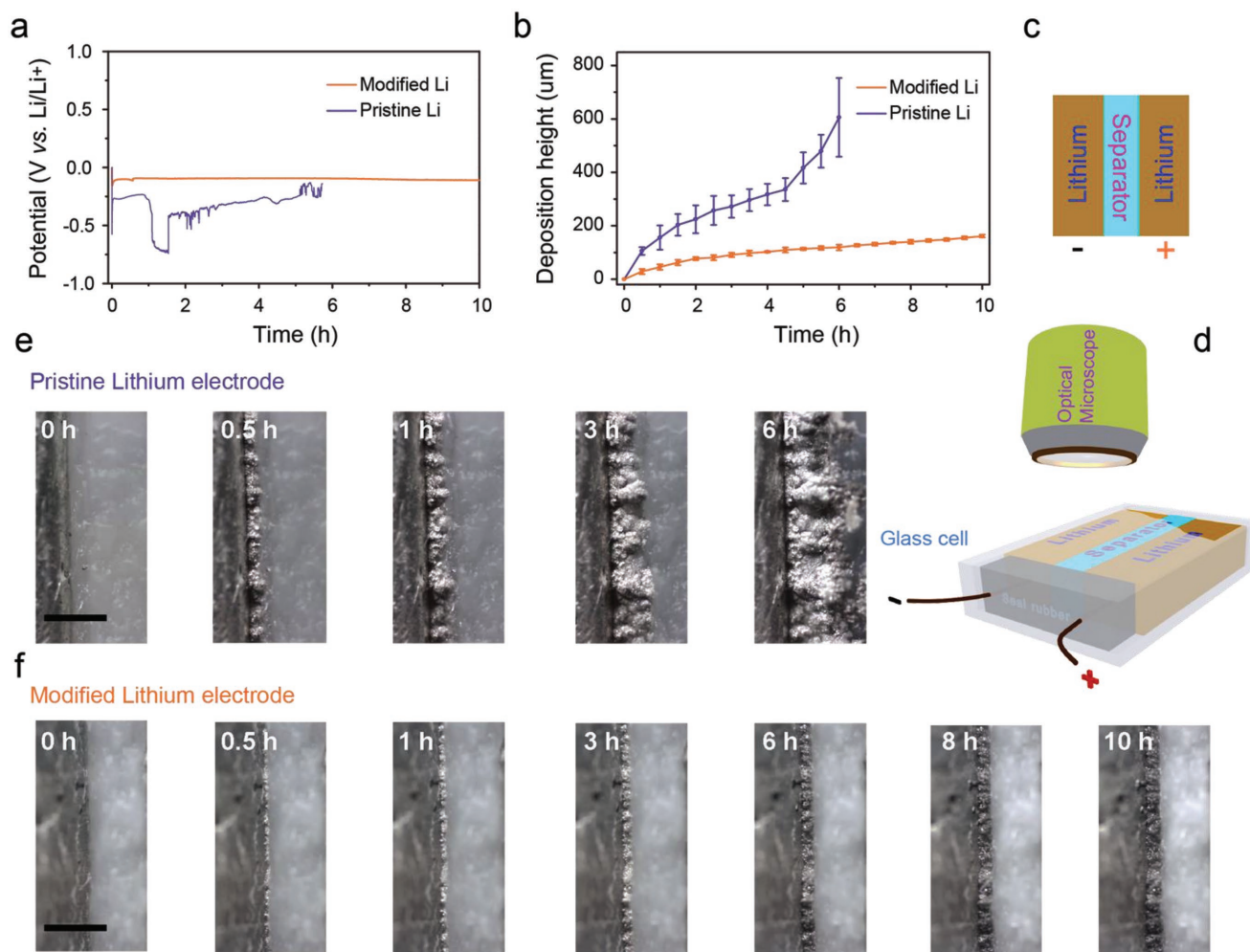
Figure 3. In situ optical microscopy observations of lithium electrochemical deposition. a) Voltage profiles of lithium deposition on pristine lithium and Li$_x$Si-modified lithium electrodes in home-made visualization glass cell at current density of 1 mA cm^{-2}; b) height of the lithium deposition as a function of time for pristine and modified lithium electrodes observed in visualization experiments; illustrator of symmetric c) battery and d) set-up for the visualization experiments; time lapse of lithium deposition on e) pristine and f) modified lithium electrodes. The scale bars for panels (e) and (f) are 500 μm. The large error bar of pristine lithium electrode in panel (b) indicates a large variation of depositing height.

plotting the height of the deposit at different times was shown in Figure 3b. The increase in the depositing thickness on the modified lithium is much slower than that on the pristine lithium as the deposited lithium on the Li$_x$Si-modified lithium foils is much denser. It is obvious that the Li$_x$Si-enriching layer results in much uniform deposition over long period of time.

Plane-view SEM images of the lithium surface shows that there is an obvious difference between the pristine and the modified lithium foil during the electrochemical process, when lithium is deposited on the surface of the pristine lithium foil (**Figure 4**a). The SEM images are false colored for greater clarity. The original images are shown in Figure S9 in the Supporting Information, lots of lithium "islands" are observed on top of the lithium with very low surface utilization of ≈22% (Figure 4d). The cause of "island deposition" boils down to the inhomogeneous surface layer on pristine lithium, which consist of the native layer of Li$_2$O, LiOH, Li$_2$CO$_3$, and so on,[68] and the as-formed SEI when in contact with the electrolyte solvents. The topographical and electrical inhomogeneity of these species on

pristine lithium results in sporadic lithium nucleation, leading to the island deposition.[69] Upon removal of lithium from the nonuniform surface (Figure 4b), the formation of pits is evident, indicating uneven removal of lithium from the surface, which is ≈15% of the total area (there is no pit observed on pristine lithium foil before electrochemical process as shown in Figure S10 in the Supporting Information.). The formation of "pits" could be attributed to the preferential dissolution at certain sites on the lithium surface, wherein the native layer is broken to create some "hot spots" with a better ionic conductivity for further lithium dissolution. Such nonuniform deposition and dissolution behavior is observed throughout cycling. It is found that ≈35% of the surface area remains inactive in the cycled electrochemical deposition (Figure 4c). Since the real local current density is largely dependent on the utilized surface area, such nonuniform deposition and dissolution behavior will increase the actual local density on the active surface during the deposition and dissolution of lithium on the pristine lithium foil, which limits high-rate performance of pristine lithium and
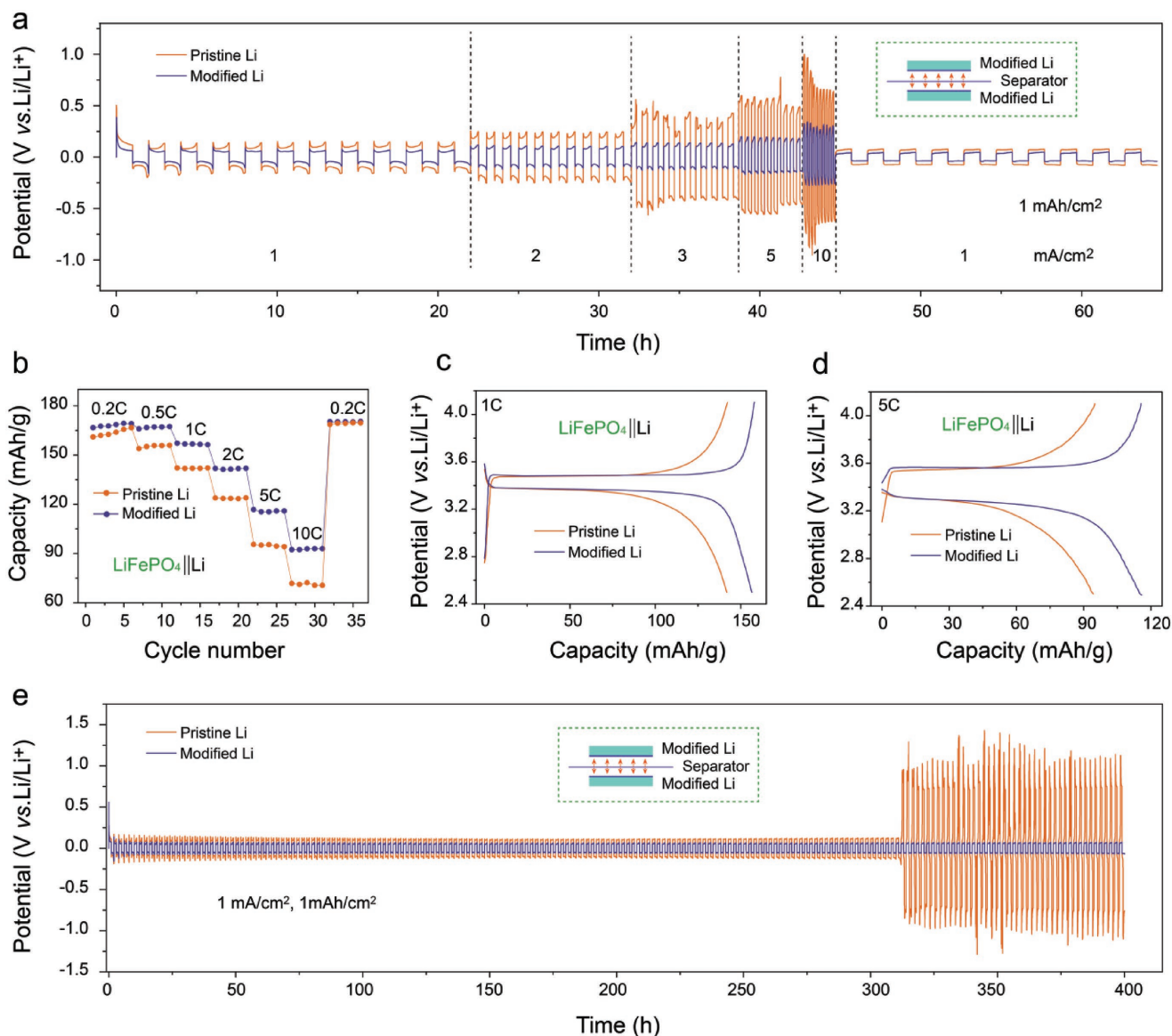
**ADVANCED
SCIENCE NEWS**
www.advancedsciencenews.com

**ADVANCED
MATERIALS**
www.advmat.de
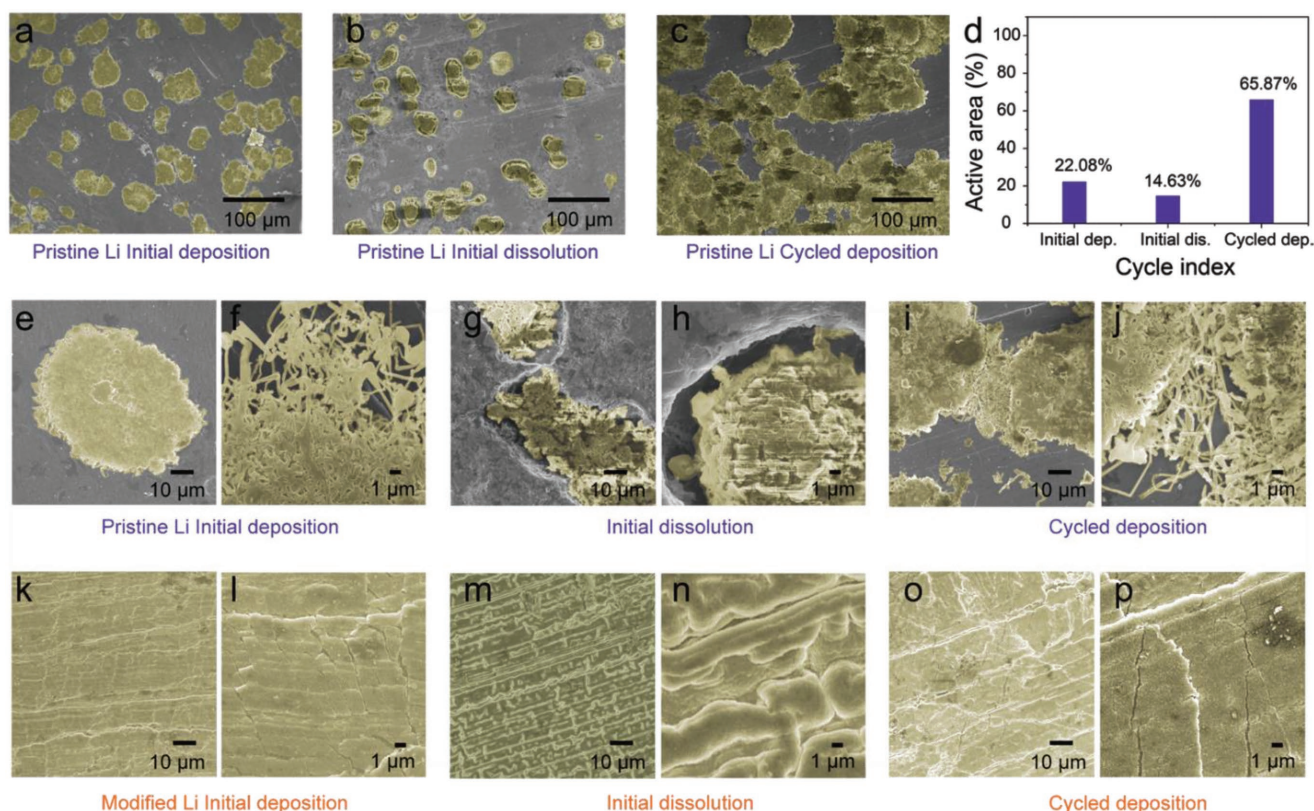
Figure 4. Microscopic studies of the electrochemical deposition and dissolution of lithium on pristine lithium foil and Li$_x$Si-modified lithium foil. SEM images of the surface of pristine lithium at the end of a) initial deposition, b) initial dissolution, and c) cycled deposition. d) Accordingly analysis of the active involved area of pristine lithium foils from the SEM images. Plane view and magnified SEM images of the surface of pristine lithium at the end of e,f) initial disposition, g,h) initial dissolution and i,j) cycled deposition. Plane view and magnified SEM images of the surface of Li$_x$Si-modified lithium foil at the end of k,l) initial disposition, m,n) initial dissolution, and o,p) cycled deposition. The dissolution and deposition current density is fixed at 1 mA cm^{-2}; and the capacity is fixed at 1 mAh cm^{-2}.

aggravate the growth of lithium dendrite. Zoom-in SEM images show that the lithium "islands" are formed by aggregation of loosened lithium dendrites (Figure 4e,f). During dissolution, the deposited lithium cannot be fully removed and deposited lithium from the previous cycles can still be observed in the pits (Figure 4g,h). Such residual lithium cannot be removed due to the poor electrical contact with the bulk lithium foil. After prolong cycling (Figure 4i,j), the dendritic lithium "islands" merge to form large "mossy" lithium plates on the surface of the pristine lithium. In contrast, the deposition and dissolution of lithium on the modified lithium foil proceed through a much more uniform manner. There is no obvious lithium dendrite observed on the surface of the Li$_x$Si-coated lithium after deposition (Figure 4k,l, the cross-section SEM images added in Figure S11 in the Supporting Information). In the case of dissolution, no pit is observed on the surface. The deposition likely goes through an initial lithiation, followed by lithium growth process (cyclic voltammetry and voltage profile of Si-deposited copper foil is shown in Figures S12 and S13 in the Supporting Information).[70] In the present case, the deposition and dissolution of lithium happens underneath the surface coating layer, while the ion-conducting alloy layer provides a uniform lithium ion flux during the deposition and dissolution (resistivity calculation of the protection film and SEM images of

the lithium deposited underneath the protection film are shown in Figures S14 and S15 in the Supporting Information, respectively). The uniform deposition and dissolution of lithium ensures that the local current density experienced by the lithium anode is same as the applied current density, in contrast to the case of pristine lithium foil where a much larger local current density is experienced on the electrode due to the limited reactive area (Figure S16, Supporting Information).

The Galvanostatic electrochemical performance of the Li$_x$Si-modified lithium foil was studied with the electrolyte of 1 M LiPF$_6$ dissolved in ethylene carbonate and diethyl carbonate (1:1 in volume) in symmetric cells. Other methods to evaluate lithium anode performance include estimation of Coulombic efficiency. While there is no consensus in the community about a standardized method yet, Zhang and co-workers have provided a good overview on the various ways for Coulombic efficiency calculations.[71] In this study, we focus on the overpotential in symmetric cells to evaluate the performance of different lithium anode structures. Due to the optimized local current density, the Li$_x$Si cell exhibits much better rate capability and cycling stability at different current densities as compared to the pristine lithium foil (**Figure 5**a). When the current density is varied from 1 to 3 mA cm^{-2}, lower overpotential from ≈40 mV (at 1 mA cm^{-2}) to ≈90 mV (at 3 mA cm^{-2}) can be obtained from

**ADVANCED
SCIENCE NEWS**

www.advancedsciencenews.com

**ADVANCED
MATERIALS**

www.advmat.de

Figure 5. Electrochemical performance of Li_xSi-modified lithium foil. a) Voltage profile of pristine lithium foil symmetric cell (orange) and that of Li_xSi-modified lithium foil symmetric cell (blue) at different rate various from 1 to 10 mA cm^{-2}. b) Rate capability and voltage profile at c) 1 C and d) 5 C of LiFePO$_4$ electrodes combined with Li_xSi-modified lithium foil (blue) and pristine lithium foil (orange); e) voltage profile of pristine lithium foil (orange) and Li_xSi-modified lithium foil symmetric cell (blue) at 1 mA cm^{-2}. Stripping/plating capacity is fixed at 1 mAh cm^{-2}, 1 C = 170 mA g^{-1}.

the Li_xSi-modified cell than those of the pristine lithium foil at the same current densities (Figure 5a). After the current density was changed back to 1 mA cm^{-2}, the overpotential of Li_xSi-modified cell decreased to ≈38 mV, indicating a good reversibility. The good rate capabilities of Li_xSi-modified lithium foil were further validated by paring with LiFeO$_4$ electrodes (mass loading ≈3.2 mg cm^{-2}). Higher capacity was constantly retained using Li_xSi-modified lithium foil as an anode through all the rates tested, especially at higher rates (Figure 5b). The LiFePO$_4$//modified lithium foil cell realized discharge capacities of 168 mAh g^{-1} at 0.2 C, 166 mAh g^{-1} at 0.5 C, 156 mAh g^{-1} at 1 C, 142 mAh g^{-1} at 2 C, 115 mAh g^{-1} at 5 C, and even 93 mAh g^{-1} at 10 C. In comparison, LiFePO$_4$//pristine lithium foil cell gave discharge capacities of 164 mAh g^{-1} at 0.2 C, 155 mAh g^{-1} at

0.5 C, 142 mAh g^{-1} at 1 C, 123 mAh g^{-1} at 2 C, 94 mAh g^{-1} at 5 C and 70 mAh g^{-1} at 10 C. The charge/discharge curves of LiFePO$_4$//modified lithium foil cells at all of the tested rates are much flatter than those of LiFePO$_4$//pristine lithium foil cells (Figure 5c,d, Figure S17 and Table S2, Supporting Information), demonstrating a very homogenous lithium deposition/dissolution processes on Li_xSi-modified lithium foil. In symmetric cells at 1 mA cm^{-2}, stable cycling with a low overpotential of ≈40 mV and flat voltage plateaus is observed for the modified lithium electrode for over 200 cycles, whereas the control pristine lithium foil suffers internal short circuit after 156 cycles (Figure 5e; according impedance studies are shown in Figure S18 in the Supporting Information.). Such a stability of Li_xSi-modified lithium foil can also be observed by

**ADVANCED
SCIENCE NEWS**

www.advancedsciencenews.com

**ADVANCED
MATERIALS**

www.advmat.de
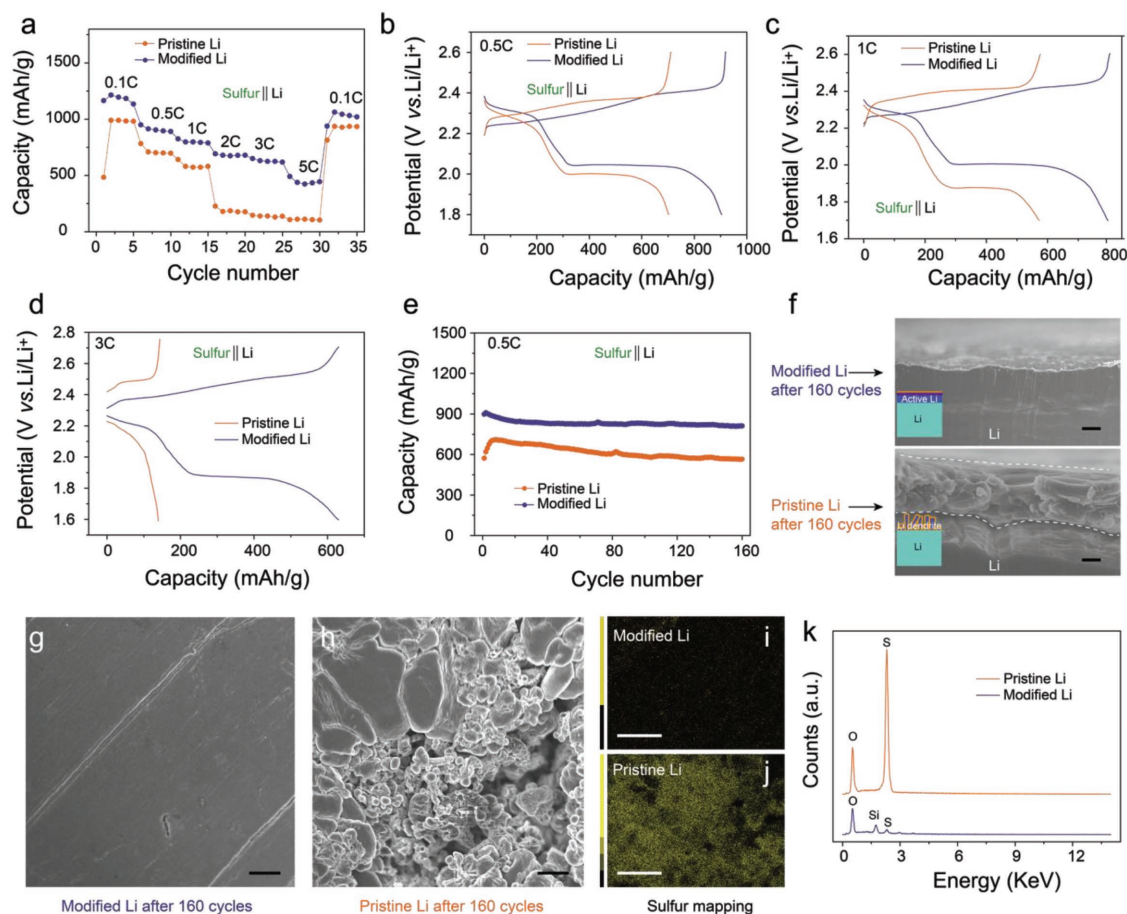
Figure 6. Effect of Li$_x$Si-enrichment in lithium–sulfur batteries. a) Rate capabilities of lithium–sulfur cells with the pristine and modified lithium anode. Voltage profiles of the lithium–sulfur batteries at b) 0.5 C, c) 1 C, and d) 3 C. e) Cycling performance of lithium–sulfur cells at 0.5 C. f) Cross-section view SEM images of modified lithium foil (upper) and pristine lithium foil (lower) after 160 cycles. Plane-view SEM images of Li$_x$Si-modified g) lithium foil and h) pristine lithium foil after 160 cycles. EDS sulfur mapping of i) modified lithium foil and j) pristine lithium foil after 160 cycles, and k) the corresponding EDS spectra. The scale bar of the intensity in panel (i) is two orders of magnitude lower than that of panel (j), indicating extremely low sulfur content on the Li$_x$Si-modified lithium foil. The scale bar is 10 µm in panels (f, g, h) and 30 µm in panels (i, j).

pairing the modified lithium with different cathode materials. When paired with LiFePO$_4$ electrodes, the cells deliver cycling capability up to 110 cycles with 100% capacity retention and an average Coulombic efficiency up to 99.7% at 0.5 C in carbonate electrolyte (Figure S19, Supporting Information; the electrochemical performance of LiFePO$_4$ electrodes with higher mass loading up to ≈7.4 mg cm^{-2} are shown in Figure S20 in the Supporting Information.).

To verify the compatibility of Li$_x$Si-modified lithium foil in lithium–sulfur batteries, Li$_x$Si-modified lithium and pristine lithium foils were further paired with high-capacity nanosulfur cathodes (mass loading of around 2 mg cm^{-2}) using an ether electrolyte.[72] As seen in **Figure 6**a, sulfur//modified lithium foil cells show a significantly higher capacity than sulfur//pristine lithium foil cells, especially at higher rates (Figure S21 and Table S2, Supporting Information). The sulfur//modified lithium foil cell realized stable discharge capacities of 1190 mAh g^{-1} at 0.1 C, 910 mAh g^{-1} at 0.5 C, 800 mAh g^{-1} at 1 C, 681 mAh g^{-1} at 2 C, 629 mAh g^{-1} at 3 C, and even 446 mAh g^{-1} at 5 C (Figure 6b–d). In comparison, sulfur//pristine lithium foil cell gave discharge capacities of 985 mAh g^{-1} at

0.1 C, 718 mAh g^{-1} at 0.5 C, 589 mAh g^{-1} at 1 C, 189 mAh g^{-1} at 2 C, 138 mAh g^{-1} at 3 C, and 107 mAh g^{-1} at 5 C. Moreover, it is clearly shown in Figure 6b–d that the Li$_x$Si-modified lithium cells exhibited lower overpotential compared with the pristine lithium foil counterpart, and a pronounced difference was observed when the rate was further increased to 3 C, wherein the pristine lithium–sulfur cell lost its second plateau and showed significant capacity drop. In contrast, the Li$_x$Si-modified lithium foil cells realized much better kinetics, with a second plateau of ≈1.9 V even at the high rate of 3 C. With nanosulfur cathode, the Li$_x$Si-modified lithium cells can be charged/discharged for up to 160 cycles with 91% capacity retention and an average Coulombic efficiency up to 99.4% at 0.5 C in ether electrolyte (Figure S22, Supporting Information; extensive cycling performance is shown in Figure S20 in the Supporting Information.). After cycling in lithium–sulfur cells, clear dendrites-like morphology can be observed from the cross-section view (Figure 6f) and plane view (Figure 6h) of the pristine lithium. A layer of porous lithium on the top of pristine lithium will increase the internal resistance of the cells, leading to low-rate capability and poor cycling performance. On the contrary, a flat

and dense lithium deposition was observed in Li_xSi-modified Li foils after long cycles (Figure 6f,g). In addition, the surface passivation of lithium foil by lithium polysulfides, which was considered as a long-standing problem in lithium–sulfur batteries, was found to be effectively mitigated by the Li_xSi coating. From the EDS analysis, much less sulfur signal was detected on the surface of the Li_xSi-modified lithium foil than that of pristine lithium foil after long cycling (Figure 6i–k; cross-sectional EDS studies are shown in Figure S23 in the Supporting Information.). The Li_xSi enrichment provides both a buffer layer in electrochemical potential between the highly reducing lithium anode and the organic electrolyte, and also uniform sites for lithiation and deposition.

Due to the high reactivity of pristine lithium metal, its surface chemistry is very complex and may include the native Li_2O, $LiOH$, Li_2CO_3, and electrochemically induced SEI species,[73] such as LiN, LiX (X = F, Cl, et al), $ROCO_2Li$, ROLi, Li_xMF_y (M = As, B,P, et al) and $RCOO_2Li$,etc. In addition to the chemical complexity, their distribution and structures also vary a lot.[67] We demonstrated that restructuring the lithium surface into Li_xSi layers improves the uniformity of lithium dissolution and deposition compared to bare lithium. The protecting layer provides a buffer between the highly reducing lithium anode and the organic electrolyte and enables uniform lithium deposition. This allows a more homogeneous utilization of lithium and a better rate capability compared with pristine lithium foil. From a safety perspective, dendritic growth on lithium foil can be effectively suppressed, as confirmed by the in situ optical microscopy (OM) and electronic microscopy studies, thus allowing the lithium anode to enjoy a long cycling life.

Experimental Section

Preparation of Li_xSi-Modified Lithium Foil: The conformal silicon deposition was carried out in an RF-magnetron sputtering system (Oerlikon 350) at room temperature. The lithium foil (99.95%, thickness: 0.59 mm) purchased from China Energy Lithium Co., Ltd., was attached on the substrate in the glove box (H_2O < 1 ppm, O_2 < 1 ppm) and then transferred into the growing chamber without exposure to the air. The system was pumped down to a background pressure of <3 × 10^{-7} mbar and then pure Ar gas was introduced to keep the working pressure at 1 × 10^{-2} mbar. A 2 inch silicon (99.99% purity) target was sputtered at 60 W for 3 h. After growth, Si-coated lithium foil was transferred into glove box, placed on an iron plate, and heated to 250 °C. After heating at 250 °C for 2 min, the Si was lithiated by the melted lithium, with surface color changing from yellow to gray. Upon cooling, the as-prepared lithium foil was pouched into disks and stored in glove box for further characterization.

Materials Characterizations: Wide-angle X-ray diffraction patterns were collected on Bruker D8 Focus Powder X-ray diffractometer using Cu Kα radiation (40 kV, 40 mA). SEM analysis was performed on JEOL-6701F SEM. Transmission electron microscopy (TEM) analysis was performed on an FEI Titan 80–300 S/TEM (scanning/transmission electron microscope) operated at 200 kV. Lithium foils at different electrochemical status (dissolution/deposition) were recovered from coil cells and transferred into SEM chamber without exposure to the air. To remove the residual electrolyte on lithium foils, the lithium foils running in carbonate electrolyte were rinsed in dimethyl carbonate for three times, while foils running in ether electrolyte were rinsed in 1,3-dioxolane. Li_xSi-modified lithium foils were cut by a dual beam focused ion beam (FIB) (Helios NanoLab NanoLab 450S) to expose the cross section for SEM characterizations. Synchrotron radiation

XPS was conducted on the SINS beamline at Singapore Synchrotron Light Source. The lithium foil was transferred into the loading chamber without exposure to the air. The available photon energy range reaches from 50 to 1200 eV. This range was covered by four spherical gratings in a modified dragon-type monochromator. At a resolving power of 2000 a photon flux of about 10^{10} photons s^{-1} 100 mA^{-1} is delivered into a spot size of 1.5 × 0.2 mm^2 (full width at half maximum).

In Situ OM Studies: A custom-made transparent glass cell was used for in situ OM studies. Symmetric configuration was used comprised of either Li_xSi-modified lithium foil or the freshly scraped lithium foils, with a piece of commercial separator filled with electrolyte placed in the middle. The electrolytes used were 1 M lithium hexafluorophosphate ($LiPF_6$, Sigma-Aldrich, battery grade, ≥99.99% trace metals basis) in 1:1 ethylene carbonate (Sigma-Aldrich, anhydrous, 99%)/diethyl carbonate (Sigma-Aldrich, anhydrous, 99%) without additives.

Electrochemical Measurement: To study the Li dissolution/deposition processes, the electrodes were assembled into CR-2032-type coin cells (MTI) in a symmetric cell. The electrodes used in symmetric configuration were either Li_xSi-modified lithium foil or the freshly scraped lithium foils (China Energy Lithium Co.,Ltd). $LiFePO_4$ powder was received from Shanghai Power Energy Storage Battery System Engineering Technology co., LTD. The $LiFePO_4$ electrodes were fabricated by mixing 70 wt% active materials, 20 wt% Super P carbon black, and 10 wt% polyvinylidene fluoride (PVDF) binders in appropriate amount of *N*-methyl-2-pyrrolidinone (NMP, Sigma-Aldrich) as solvent. After stirring for 8 h, the resulting paste was spread on aluminum foil by Automatic Film Coater with Vacuum Pump and Micrometer Doctor Blade (MTI). After evaporation of NMP solvent in a vacuum oven at 120 °C for 12 h, the electrodes were pressed and cut into disks. Nanosulfur was synthesized according to previous report.[72] Sulfur working electrode was fabricated by mixing Super P carbon black (30 wt%) and PVDF (10 wt %) binder with the nanosulfur (60 wt%) in NMP to form a slurry. The slurry was then coated onto carbon coated aluminum foil and dried under vacuum overnight at 40 °C. Li_xSi-modified lithium foil or pristine lithium foil was then paired with $LiFePO_4$/nanosulfur electrodes to evaluate the electrochemical performance by using CR-2032 cell. The electrolytes used were 1 M lithium hexafluorophosphate ($LiPF_6$, Sigma-Aldrich, battery grade, ≥99.99% trace metals basis) in 1:1 ethylene carbonate (Sigma-Aldrich, anhydrous, 99%) /diethyl carbonate (Sigma-Aldrich, anhydrous, 99%) without additives. The electrolytes used for sulfur//lithium foil cells were 1.0 M lithium *bis*(trifluoromethanesulfonyl)imide (LiTFSI, Sigma-Aldrich, 99.95% trace metals basis) and 0.1 M $LiNO_3$ (Sigma-Aldrich, 99.99% trace metals basis) in 1,3-dioxolane (Sigma-Aldrich, anhydrous, 99.8%) and 1,2-dimethoxyethane (Sigma-Aldrich, anhydrous, 99.5%) (volume ratio, 1:1). Those cells were tested on a LAND 8-channel battery tester. Electrochemical impedance spectroscopy was carried out using Autolab PGSTAT30 digital potentiostat/galvanostat at room temperature about 23 °C. The frequency was varied from 0.1 MHz to 10 mHz with an alternating voltage signal amplitude of 10 mV.

Supporting Information

Supporting Information is available from the Wiley Online Library or from the author.

Acknowledgements

Conflict of Interest

The authors declare no conflict of interest.

Keywords

[1] M. D. Tikekar, S. Choudhury, Z. Tu, L. A. Archer, *Nat. Energy* **2016**, *1*, 16114.

[2] W. Xu, J. Wang, F. Ding, X. Chen, E. Nasybulin, Y. Zhang, J.-G. Zhang, *Energy Environ. Sci.* **2014**, *7*, 513.

[3] D. Lin, Y. Liu, Y. Cui, *Nat. Nanotechnol.* **2017**, *12*, 194.

[4] Y. Guo, H. Li, T. Zhai, *Adv. Mater.* **2017**, *29*, 1700007.

[5] L. Suo, Y.-S. Hu, H. Li, M. Armand, L. Chen, *Nat. Commun.* **2013**, *4*, 1481.

[6] J. M. Tarascon, M. Armand, *Nature* **2001**, *414*, 359.

[7] D. S. Jung, M.-H. Ryou, Y. J. Sung, S. B. Park, J. W. Choi, *Proc. Natl. Acad. Sci. USA* **2013**, *110*, 12229.

[8] C. Yang, K. Fu, Y. Zhang, E. Hitz, L. Hu, *Adv. Mater.* **2017**, *29*, 1701169.

[9] P. G. Bruce, S. A. Freunberger, L. J. Hardwick, J.-M. Tarascon, *Nat. Mater.* **2012**, *11*, 19.

[10] Z. Gao, H. Sun, L. Fu, F. Ye, Y. Zhang, W. Luo, Y. Huang, *Adv. Mater.* **2018**, *30*, 1705702.

[11] X. Liu, J.-Q. Huang, Q. Zhang, L. Mai, *Adv. Mater.* **2017**, *29*, 1601759.

[12] Y. Liu, Q. Liu, L. Xin, Y. Liu, F. Yang, E. A. Stach, J. Xie, *Nat. Energy* **2017**, *2*, 17083.

[13] D. Aurbach, B. D. McCloskey, L. F. Nazar, P. G. Bruce, *Nat. Energy* **2016**, *1*, 16128.

[14] R. Bhattacharyya, B. Key, H. Chen, A. S. Best, A. F. Hollenkamp, C. P. Grey, *Nat. Mater.* **2010**, *9*, 504.

[15] P. Bai, J. Li, F. R. Brushett, M. Z. Bazant, *Energy Environ. Sci.* **2016**, *9*, 3221.

[16] D. Lu, Y. Shao, T. Lozano, W. D. Bennett, G. L. Graff, B. Polzin, J. Zhang, M. H. Engelhard, N. T. Saenz, W. A. Henderson, P. Bhattacharya, J. Liu, J. Xiao, *Adv. Energy Mater.* **2015**, *5*, 1400993.

[17] Q. Li, S. Tan, L. Li, Y. Lu, Y. He, *Sci. Adv.* **2017**, *3*, e1701246.

[18] K. Xu, *Chem. Rev.* **2014**, *114*, 11503.

[19] G. Rong, X. Zhang, W. Zhao, Y. Qiu, M. Liu, F. Ye, Y. Xu, J. Chen, Y. Hou, W. Li, W. Duan, Y. Zhang, *Adv. Mater.* **2017**, *29*, 1606187.

[20] Y. S. Cohen, Y. Cohen, D. Aurbach, *J. Phys. Chem. B* **2000**, *104*, 12282.

[21] X.-B. Cheng, R. Zhang, C.-Z. Zhao, F. Wei, J.-G. Zhang, Q. Zhang, *Adv. Sci.* **2016**, *3*, 1500213.

[22] R. L. Sacci, J. M. Black, N. Balke, N. J. Dudney, K. L. More, R. R. Unocic, *Nano Lett.* **2015**, *15*, 2011.

[23] X.-B. Cheng, T.-Z. Hou, R. Zhang, H.-J. Peng, C.-Z. Zhao, J.-Q. Huang, Q. Zhang, *Adv. Mater.* **2016**, *28*, 2888.

[24] M.-H. Ryou, Y. M. Lee, Y. Lee, M. Winter, P. Bieker, *Adv. Funct. Mater.* **2015**, *25*, 834.

[25] H. Wang, D. Lin, Y. Liu, Y. Li, Y. Cui, *Sci. Adv.* **2017**, *3*, e1701301.

[26] X. Liang, Q. Pang, I. R. Kochetkov, M. S. Sempere, H. Huang, X. Sun, L. F. Nazar, *Nat. Energy* **2017**, *2*, 17119.

[27] Q. Yun, Y.-B. He, W. Lv, Y. Zhao, B. Li, F. Kang, Q.-H. Yang, *Adv. Mater.* **2016**, *28*, 6932.

[28] S.-H. Wang, Y.-X. Yin, T.-T. Zuo, W. Dong, J.-Y. Li, J.-L. Shi, C.-H. Zhang, N.-W. Li, C.-J. Li, Y.-G. Guo, *Adv. Mater.* **2017**, *29*, 1703729.

[29] L.-L. Lu, J. Ge, J.-N. Yang, S.-M. Chen, H.-B. Yao, F. Zhou, S.-H. Yu, *Nano Lett.* **2016**, *16*, 4431.

[30] C.-P. Yang, Y.-X. Yin, S.-F. Zhang, N.-W. Li, Y.-G. Guo, *Nat. Commun.* **2015**, *6*, 8058.

[31] S. S. Zhang, X. Fan, C. Wang, *Electrochim. Acta* **2017**, *258*, 1201.

[32] R. Zhang, X.-B. Cheng, C.-Z. Zhao, H.-J. Peng, J.-L. Shi, J.-Q. Huang, J. Wang, F. Wei, Q. Zhang, *Adv. Mater.* **2016**, *28*, 2155.

[33] A. Zhamu, G. Chen, C. Liu, D. Neff, Q. Fang, Z. Yu, W. Xiong, Y. Wang, X. Wang, B. Z. Jang, *Energy Environ. Sci.* **2012**, *5*, 5701.

[34] G. Zheng, S. W. Lee, Z. Liang, H. W. Lee, K. Yan, H. Yao, H. Wang, W. Li, S. Chu, Y. Cui, *Nat. Nanotechnol.* **2014**, *9*, 618.

[35] H. Ye, S. Xin, Y.-X. Yin, J.-Y. Li, Y.-G. Guo, L.-J. Wan, *J. Am. Chem. Soc.* **2017**, *139*, 5916.

[36] R. Mukherjee, A. V. Thomas, D. Datta, E. Singh, J. Li, O. Eksik, V. B. Shenoy, N. Koratkar, *Nat. Commun.* **2014**, *5*, 3710.

[37] S. Liu, A. Wang, Q. Li, J. Wu, K. Chiou, J. Huang, J. Luo, *Joule* **2018**, *2*, 184.

[38] D. Lin, Y. Liu, Z. Liang, H.-W. Lee, J. Sun, H. Wang, K. Yan, J. Xie, Y. Cui, *Nat. Nanotechnol.* **2016**, *11*, 626.

[39] Y. Liu, D. Lin, Z. Liang, J. Zhao, K. Yan, Y. Cui, *Nat. Commun.* **2016**, *7*, 10992.

[40] C. Wang, Y. Gong, B. Liu, K. Fu, Y. Yao, E. Hitz, Y. Li, J. Dai, S. Xu, W. Luo, E. D. Wachsman, L. Hu, *Nano Lett.* **2017**, *17*, 565.

[41] J. Zheng, M. H. Engelhard, D. Mei, S. Jiao, B. J. Polzin, J.-G. Zhang, W. Xu, *Nat. Energy* **2017**, *2*, 17012.

[42] L. Suo, W. Xue, M. Gobet, S. G. Greenbaum, C. Wang, Y. Chen, W. Yang, Y. Li, J. Li, *Proc. Natl. Acad. Sci. USA* **2018**, *115*, 1156.

[43] G. Ma, Z. Wen, M. Wu, C. Shen, Q. Wang, J. Jin, X. Wu, *Chem. Commun.* **2014**, *50*, 14209.

[44] N. J. Dudney, *J. Power Sources* **2000**, *89*, 176.

[45] D. Lin, Y. Liu, W. Chen, G. Zhou, K. Liu, B. Dunn, Y. Cui, *Nano Lett.* **2017**, *17*, 3731.

[46] X. Han, Y. Gong, K. Fu, X. He, G. T. Hitz, J. Dai, A. Pearse, B. Liu, H. Wang, G. Rubloff, Y. Mo, V. Thangadurai, E. D. Wachsman, L. Hu, *Nat. Mater.* **2017**, *16*, 572.

[47] W. Li, H. Yao, K. Yan, G. Zheng, Z. Liang, Y.-M. Chiang, Y. Cui, *Nat. Commun.* **2015**, *6*, 7436.

[48] X. Yu, J. B. Bates, G. E. Jellison, F. X. Hart, *J. Electrochem. Soc.* **1997**, *144*, 524.

[49] K. Fu, Y. Gong, B. Liu, Y. Zhu, S. Xu, Y. Yao, W. Luo, C. Wang, S. D. Lacey, J. Dai, Y. Chen, Y. Mo, E. Wachsman, L. Hu, *Sci. Adv.* **2017**, *3*, e1601659.

[50] M. D. Tikekar, L. A. Archer, D. L. Koch, *Sci. Adv.* **2016**, *2*, e1600320.

[51] Y. Lu, Z. Tu, L. A. Archer, *Nat. Mater.* **2014**, *13*, 961.

[52] Y. Lu, K. Korf, Y. Kambe, Z. Tu, L. A. Archer, *Angew. Chem., Int. Ed.* **2014**, *53*, 488.

[53] C.-Z. Zhao, X.-Q. Zhang, X.-B. Cheng, R. Zhang, R. Xu, P.-Y. Chen, H.-J. Peng, J.-Q. Huang, Q. Zhang, *Proc. Natl. Acad. Sci. USA* **2017**, *114*, 11069.

[54] W. Zhou, S. Wang, Y. Li, S. Xin, A. Manthiram, J. B. Goodenough, *J. Am. Chem. Soc.* **2016**, *138*, 9385.

[55] C. Yang, B. Liu, F. Jiang, Y. Zhang, H. Xie, E. Hitz, L. Hu, *Nano Res.* **2017**, *10*, 4256.

[56] B. Zhu, Y. Jin, X. Hu, Q. Zheng, S. Zhang, Q. Wang, J. Zhu, *Adv. Mater.* **2016**, *29*, 1603755.

[57] G. A. Umeda, E. Menke, M. Richard, K. L. Stamm, F. Wudl, B. Dunn, *J. Mater. Chem.* **2011**, *21*, 1593.

[58] J. Luo, R.-C. Lee, J.-T. Jin, Y.-T. Weng, C.-C. Fang, N.-L. Wu, *Chem. Commun.* **2017**, *53*, 963.

[59] X.-X. Zeng, Y.-X. Yin, N.-W. Li, W.-C. Du, Y.-G. Guo, L.-J. Wan, *J. Am. Chem. Soc.* **2016**, *138*, 15825.

**ADVANCED
SCIENCE NEWS**

www.advancedsciencenews.com

**ADVANCED
MATERIALS**

www.advmat.de

[60] H. Lee, J. Song, Y.-J. Kim, J.-K. Park, H.-T. Kim, *Sci. Rep.* **2016**, *6*, 30830.

[61] R. Khurana, J. L. Schaefer, L. A. Archer, G. W. Coates, *J. Am. Chem. Soc.* **2014**, *136*, 7395.

[62] Y. Gao, Y. Zhao, Y. C. Li, Q. Huang, T. E. Mallouk, D. Wang, *J. Am. Chem. Soc.* **2017**, *139*, 15288.

[63] S. Choudhury, Z. Tu, S. Stalin, D. Vu, K. Fawole, D. Gunceler, R. Sundararaman, L. A. Archer, *Angew. Chem., Int. Ed.* **2017**, *56*, 13070.

[64] A. C. Kozen, C.-F. Lin, A. J. Pearse, M. A. Schroeder, X. Han, L. Hu, S.-B. Lee, G. W. Rubloff, M. Noked, *ACS Nano* **2015**, *9*, 5884.

[65] J.-S. Kim, D. W. Kim, H. T. Jung, J. W. Choi, *Chem. Mater.* **2015**, *27*, 2780.

[66] K. Yan, H.-W. Lee, T. Gao, G. Zheng, H. Yao, H. Wang, Z. Lu, Y. Zhou, Z. Liang, Z. Liu, S. Chu, Y. Cui, *Nano Lett.* **2014**, *14*, 6016.

[67] D. Aurbach, *J. Power Sources* **2000**, *89*, 206.

[68] X.-B. Cheng, R. Zhang, C.-Z. Zhao, Q. Zhang, *Chem. Rev.* **2017**, *117*, 10403.

[69] A. Pei, G. Zheng, F. Shi, Y. Li, Y. Cui, *Nano Lett.* **2017**, *17*, 1132.

[70] K. Yan, Z. Lu, H.-W. Lee, F. Xiong, P.-C. Hsu, Y. Li, J. Zhao, S. Chu, Y. Cui, *Nat. Energy* **2016**, *1*, 16010.

[71] B. D. Adams, J. Zheng, X. Ren, W. Xu, J.-G. Zhang, *Adv. Energy Mater.* **2017**, *8*, 1702097.

[72] W. Li, G. Zheng, Y. Yang, Z. W. Seh, N. Liu, Y. Cui, *Proc. Natl. Acad. Sci. USA* **2013**, *110*, 7148.

[73] E. Peled, *J. Electrochem. Soc.* **1979**, *126*, 2047.